Chlamydomonas reinhardtii formin and profilin are optimized for acute rapid actin filament assembly

Jenna R. Christensen[a], Michael J. Glista[a], David M. Mueller[b], Yujie Li[a], Jennifer A. Sees[a], Colleen T. Skau[a], Laurens J. Mets[a], Prachee Avasthi[b,c*], and David R. Kovar[a,d*]

[a]Department of Molecular Genetics and Cell Biology
The University of Chicago, Chicago, IL 60637, USA
[b]Department of Anatomy and Cell Biology
University of Kansas Medical Center, Kansas City, KS 66103
[c]Department of Ophthalmology
University of Kansas Medical Center, Kansas City, KS 66103
[d]Department of Biochemistry and Molecular Biology
The University of Chicago, Chicago, IL 60637, USA

*Co-corresponding authors

Address correspondence to:

Prachee Avasthi
3901 Rainbow Boulevard
MS 3051, 2089 HLSIC
Kansas City KS 66103

E-mail: pavasthi@kumc.edu
Phone: 913-588-7344

David R. Kovar
The University of Chicago
920 East 58th Street
CLSC Suite 915E
Chicago, IL 60637

E-mail: drkovar@uchicago.edu
Phone: 773-834-2810

Running title: *Chlamydomonas* formin CrFor1
Key words: *Chlamydomonas reinhardtii,* actin, formin, profilin

Abbreviations: LatB, latrunculin B; CrPRF, *Chlamydomonas reinhardtii* profilin; CrFor1, *Chlamydomonas reinhardtii* formin 1; PRR, proline rich region; TIRF, total internal reflection fluorescence

SUMMARY STATEMENT

Chlamydomonas reinhardtii formin CrFor1 initiates rapid actin filament assembly of actin monomers associated with actin assembly inhibitor profilin CrPRF.

ABSTRACT

Chlamydomonas reinhardtii is a unicellular green alga that appears less dependent upon a conventional actin cytoskeleton than other eukaryotes, in part due to overlapping functions of a second non-conventional actin. One network that contains exclusively conventional F-actin is the fertilization tubule, a mating structure at the apical cell surface in gametes. Therefore, *Chlamydomonas* is an excellent system to investigate how actin polymerization is regulated in space and time. *Chlamydomonas* expresses a profilin (CrPRF), and a formin (CrFor1) that we have characterized for the first time. We found that unlike typical profilins, CrPRF prevents unwanted actin assembly by strongly inhibiting both F-actin nucleation and barbed end elongation at equimolar concentrations to actin. However, CrFor1 is able to stimulate rapid actin filament assembly of CrPRF-bound actin. CrPRF further favors CrFor1-mediated actin assembly by potently inhibiting Arp2/3 complex-mediated actin assembly. The small molecule formin inhibitor SMIFH2 prevents fertilization tubule formation in gametes, suggesting that mating is a primary function of CrFor1. Together, these findings indicate that CrFor1 and CrPRF cooperate to selectively and rapidly assemble F-actin at the right time and place.

INTRODUCTION

The actin cytoskeleton is a dynamic system important for diverse cellular processes. *Chlamydomonas reinhardtii* expresses a single conventional actin, IDA5, with 90% identity to mammalian actin, as well as an unconventional actin, NAP1 (Kato-Minoura, 1998; Lee et al., 1997), with low identity to mammalian actin (64%). Despite two actin genes, few F-actin networks have been identified in *Chlamydomonas*. An anti-actin antibody revealed actin surrounding the nucleus during interphase (Harper et al., 1992). This actin relocalizes throughout the cell cycle, moving from the anterior of the cell

during preprophase and metaphase to the cleavage furrow during cytokinesis (Harper et al., 1992). The antibody-labeled actin networks are not stained by the fluorescent phallotoxin phallicidin (Harper et al., 1992), possibly because they are either composed of actin monomers or because the structure or dynamics of cytoplasmic filaments cannot support binding of phallotoxins, as in apicomplexican parasites (Schmitz et al., 2005; Skillman et al., 2011). Furthermore, actin depolymerizing Latrunculin B (LatB) drug treatment does not inhibit cell division (Kato-Minoura et al., 1997). While this may appear to confirm that cleavage furrow localized actin is monomeric, cytokinesis may instead utilize LatB-insensitive NAP1 (Onishi et al., 2016), which is upregulated during LatB treatment. Direct F-actin labeling using the fluorescent Lifeact peptide also showed perinuclear localization during interphase (Avasthi et al., 2014). This perinuclear pool of F-actin is lost upon LatB treatment, but is replaced by what are likely Lifeact-binding NAP1 filaments within 1 hour (Onishi et al., 2016). F-actin also localizes at the base of the flagella, where it is important for intraflagellar transport (Avasthi et al., 2014). However, the nature of this F-actin network awaits further characterization.

One clearly defined F-actin network in *Chlamydomonas* is the fertilization tubule. The fertilization tubule is an F-actin-rich structure found in mating type + gametes (Detmers et al., 1985; Detmers et al., 1983), which during mating protrudes from the 'doublet zone', a region between the two flagella (Detmers et al., 1983). Phallicidin staining of F-actin strongly labels fertilization tubules (Detmers et al., 1985), and isolation of fertilization tubules have revealed actin as a major component (Wilson et al., 1997). Additionally, null mutants lacking conventional actin cannot form fertilization tubules (Kato-Minoura, 1998). The context-dependent formation of this well-defined F-actin structure in *Chlamydomonas* provides an exceptional opportunity to understand how a cell is capable of precisely regulating its actin cytoskeleton so that actin polymerization occurs only at a very specific place and time.

Chlamydomonas expresses a profilin (CrPRF) that, like other profilins, inhibits the nucleation of actin monomers and therefore presumably prevents unwanted actin assembly (Kovar et al., 2001). We have identified a *Chlamydomonas* formin (CrFor1) actin assembly factor, which has not been characterized and its cellular role in *Chlamydomonas* not yet determined. Therefore, we sought to characterize the formin

CrFor1 and determine how CrFor1 assembles actin monomers bound to CrPRF. Additionally, we wished to determine the role of CrFor1 in *Chlamydomonas* cells. We found that in addition to inhibiting nucleation, CrPRF potently inhibits the barbed end elongation of actin filaments at relatively low concentrations. However, CrFor1 overcomes this inhibition and swiftly assembles CrPRF-bound actin monomers in to actin filaments that elongate rapidly. Additionally, we found that *Chlamydomonas* cells treated with the formin inhibitor SMIFH2 do not form fertilization tubules, suggesting that the collective activities of CrPRF and CrFor1 regulate acute F-actin assembly for mating in *Chlamydomonas*.

RESULTS

CrPRF inhibits nucleation and elongation of actin filaments

In cells, the majority of unassembled G-actin is bound to profilin (Carlsson et al., 1977; Kaiser et al., 1999; Lu and Pollard, 2001). Profilin inhibits the nucleation of new actin filaments, but once an actin filament has been formed, profilin-bound actin monomers add to the barbed end of growing actin filaments to essentially the same degree as free monomers (Pollard and Cooper, 1984). Additionally, mammalian profilins promote nucleotide exchange (such as ADP to ATP) of actin, though plant profilins do not (Goldschmidt-Clermont et al., 1991; Mockrin and Korn, 1980; Perelroizen et al., 1996; Perelroizen et al., 1994).

Chlamydomonas profilin CrPRF is found throughout the cytoplasm and flagellar compartments of the cell, but is enriched at the base of the flagella in vegetative cells and below the fertilization tubule in mating type + gametes (Kovar et al., 2001). Previous work showed that unlike typical profilins, CrPRF inhibits the nucleotide exchange of bound G-actin. CrPRF might therefore inhibit actin assembly in cells more potently than other profilins, potentially explaining the lack of abundant F-actin networks in *Chlamydomonas*. We confirmed that the spontaneous assembly of actin monomers was inhibited by CrPRF in a concentration-dependent manner (Fig. 1A), like other profilins including fission yeast SpPRF, revealing a relatively high affinity for actin monomers (K_d=0.14 µM). Surprisingly, by directly observing the spontaneous assembly of 1.5 µM

Mg-ATP actin monomers using Total Internal Reflection Fluorescence (TIRF) microscopy, we found that unlike other profilins such as SpPRF, CrPRF also significantly inhibits the barbed end elongation of actin filaments at concentrations where the ratio of CrPRF to actin is equal or only 2- to 3-fold higher (Fig. 1B). Therefore, CrPRF is a multi-faceted inhibitor of actin polymerization that potently prevents both actin filament nucleation and elongation.

As actin filament formation in *Chlamydomonas* appears to be extremely limited, an inhibitory profilin such as CrPRF is ideal to prevent unwanted spontaneous actin assembly. However, as F-actin is present within the fertilization tubule during mating, F-actin polymerization must be facilitated at the correct time and place. Therefore, we speculated that an actin assembly factor such as a formin is responsible for rapid actin assembly at fertilization tubule sites.

Identification of a formin in *Chlamydomonas reinhardtii*

A BLAST search for conserved formin FH2 domain lasso and post sequences using mouse formin (CAA37668 – aa 986-1251) as query identified a single *Chlamydomonas* gene locus (Cre03.g166700 in the version 5.5 genome assembly) as a candidate formin. Manual inspection of the genome region upstream of the lasso element revealed an FH1 domain containing at least three proline rich repeats (PRRs) in the same reading frame with typical 6-8aa spacing between. An additional 7 PRRs with typical short (8-12aa) spacing were found further upstream of an unusually long spacer of 37 amino acids. A Kazusa DNA Research Institute EST sequence from *Chlamydomonas* (HCL081g04) confirmed splicing of the putative FH2 domain to the first three PRRs of the FH1 domain. A full length cDNA sequence provided by Susan Dutcher (personal communication) confirmed expression of the long spacer and all 10 PRR regions within a 2959 aa protein (Fig. 2A). We created bacterial expression constructs containing both 3 and 10 PRRs along with the FH2 domain and confirmed their ability to stimulate actin polymerization (Fig. 2), suggesting that the expressed protein is a formin. This formin was named *Chlamydomonas reinhardtii* formin 1 (CrFor1).

CrFor1 efficiently nucleates but weakly elongates actin filaments

Formins are a conserved family of actin assembly factors that nucleate actin filaments and then increase the elongation rate, in the presence of profilin, by remaining processively associated with the barbed end (Breitsprecher and Goode, 2013). Formins contain actin assembly FH1 and FH2 domains, which are typically flanked by regulatory regions. Functional formins are dimers, with two FH2 domains interacting head-to-tail to create a donut-shaped dimer capable of creating a stable actin 'nucleus' (Otomo et al., 2005). In addition, the FH2 dimer maintains processive association with the elongating barbed end of an actin filament (Kovar, 2006). The unstructured FH1 domains are rich in PRRs that bind to profilin and promote rapid association of profilin-actin with the barbed end of an elongating filament. In order to investigate the actin assembly properties of the formin CrFor1, we created a set of constructs containing the CrFor1 FH1 and FH2 domains, alone or in combination (Fig. 2A).

CrFor1's capacity to stimulate actin assembly was initially investigated by measuring the effect of CrFor1 on actin polymerization over time using spontaneous pyrene actin assembly assays. CrFor1 containing the FH2 alone (CrFor1(FH2)) or both the FH1 and FH2 domains (CrFor1(3P,FH2) and CrFor1(10P,FH2), hereafter referred to as CrFor1(FH1,FH2)), all stimulate actin assembly in a nearly identical concentration-dependent manner (Fig. 2B-C), and more potently than a well-characterized control formin fission yeast Cdc12(FH1,FH2) (Fig. 2B-C) (Kovar et al., 2003; Scott et al., 2011). Though these results indicate that CrFor1 increases the overall rate of actin polymerization, spontaneous pyrene actin assembly assays are unable to differentiate between an increase in the nucleation and/or elongation of actin filaments.

To differentiate between the contributions of nucleation and elongation to the overall enhanced polymerization rate, we first examined the effect of CrFor1 on actin filament elongation using seeded pyrene actin assembly assays. In the presence of actin filament seeds, elongation of the seeds dominates the reaction and the contribution of nucleation to the overall actin polymerization rate is eliminated. Addition of CrFor1(FH2), CrFor1(3P,FH2) and CrFor1(FH1,FH2) to seeded assembly reactions all reduced the actin assembly rate in a concentration dependent matter (Fig. 2D-E), suggesting that CrFor1 inhibits actin filament elongation, and that the increased actin assembly rate observed in spontaneous pyrene actin assays is due to CrFor1-mediated

nucleation. Fits of the initial seeded polymerization rates over a range of formin concentrations revealed dissociation rate constants (K_d) for actin filament barbed ends in the low nanomolar range: CrFor1(FH2) (K_d=1.6 nM), CrFor1(3P,FH2) (K_d=0.17 nM), CrFor1(FH1,FH2) (K_d=0.24 nM), and Cdc12(FH1,FH2) (K_d=0.33 nM) (Fig. 2E).

Similarly, in the presence of CrFor1 Fh1 and FH2 fragments, the rate of F-actin depolymerization upon dilution to the critical concentration was significantly reduced over a range of their concentrations (Fig. 2F-G). Curve fits revealed affinities (K_d) for actin filament barbed ends similar to those determined by seeded assembly: CrFor1(FH2) (K_d=0.40 nM), CrFor1(3P,FH2) (K_d=0.40 nM), CrFor1(FH1,FH2) (K_d=0.68 nM), and Cdc12(FH1,FH2) (K_d=0.76 nM) (Fig. 2G). Together, these results indicate that CrFor1 potently stimulates actin nucleation, while inhibiting actin filament elongation. In addition, like other formins, CrFor1 binds actin filament barbed ends with an affinity in the low nanomolar range.

Fission yeast profilin SpPRF enhances CrFor1-mediated actin assembly

We found that in the absence of profilin, *Chlamydomonas* formin CrFor1 has potent nucleation activity but also significantly inhibits actin filament barbed end elongation, similar to the fission yeast formin Cdc12. However, like other formins (Kovar et al., 2006), Cdc12-associated filaments elongate their barbed ends ~30-fold faster when fission yeast profilin SpPRF is included in the reaction (Kovar et al., 2003; Scott et al., 2011), and presumably profilin will also increase the elongation rate of filaments nucleated by CrFor1. We first tested the ability of profilins CrPRF and SpPRF to bind to the FH1 domains of CrFor1 and Cdc12. Interestingly, although CrPRF binds much more weakly than SpPRF to non-physiological poly-L-proline (Fig. 3A, C) (Kovar et al., 2001), CrPRF and SpPRF have similar affinities for the FH1 domains of both CrFor1 and Cdc12 (Fig. 3B,C), all with dissociation rate constants (K_d) within the low micromolar range.

Although CrPRF binds well to the CrFor1 FH1 domain, the capacity of a formin to add profilin-actin to filament barbed ends depends on complementary interactions with profilin and both the FH1 and FH2 domains of the formin (Bestul et al., 2015; Neidt et al., 2009). We initially tested the ability of CrFor1 to assemble SpPRF-actin, as SpPRF

is widely compatible with different formin isoforms (Bestul et al., 2015; Neidt et al., 2009). Spontaneous pyrene actin assembly assays revealed that CrFor1 constructs containing both the FH1 and FH2 domains (CrFor1(3P,FH2) and CrFor1(FH1,FH2)) rapidly accelerate actin assembly in the presence of SpPRF (Fig. 3D-E). Conversely, SpPRF inhibits actin assembly by CrFor1(FH2), the construct lacking the FH1 domain (Fig. 3D-E). The pyrene actin assembly rates measured for CrFor1(3P,FH2) and CrFor1(FH1,FH2) are significantly greater than those of Cdc12(FH1,FH2) over a range of SpPRF concentrations (Fig. 3E), suggesting that SpPRF dramatically increases the processive barbed end elongation rate of CrFor1-nucleated actin filaments.

CrPRF-actin is utilized specifically by CrFor1

We next examined the ability of CrFor1 to assemble actin monomers bound to CrPRF. In spontaneous pyrene actin assembly assays, the pyrene fluorescence measured in reactions containing CrFor1 and CrPRF is sharply reduced relative to actin alone or actin in the presence of CrFor1 (Fig. 3F). While this could indicate that CrPRF severely inhibits CrFor1-mediated actin assembly, it is also possible that the combination of CrFor1 and CrPRF prevents assembly of actin labeled on Cys-374 with pyrene, as we have described for other formin and profilin combinations (Kovar et al., 2006; Scott et al., 2011). Therefore, we directly visualized actin filaments formed in spontaneous pyrene actin assembly assays in the presence of different combinations of formin and profilin. After assembling for 600 seconds, the bulk polymerization reactions were stopped by diluting into TRITC-Phalloidin to allow visualization of filaments by fluorescence microscopy (Fig. 3G). In the absence of profilin, CrFor1 produces many small actin filaments (average length, 2.7 ± 4.0 µm), indicative of efficient nucleation by CrFor1, as suggested by spontaneous pyrene actin assembly assays (Fig. 2). Additionally, CrFor1 facilitates formation of long actin filaments in the presence of both SpPRF (16.6 ± 10.2 µm) and CrPRF (27.4 ± 17.5 µm). Interestingly, although CrFor1 can utilize either SpPRF or CrPRF to elongate actin filaments, Cdc12 is unable to form long filaments in the presence of CrPRF (average length, 4.2 ± 4.9 µm) (Fig. 3G), suggesting that CrPRF is tailored for elongation by CrFor1. Together, these results indicate that CrFor1 is capable of efficient actin filament nucleation, and in the presence

of its complimentary profilin CrPRF, rapidly elongates these filaments. In addition, the inability of Cdc12 to elongate CrPRF-associated actin suggests that CrFor1 and CrPRF are tailored to precisely and rapidly polymerize F-actin.

CrFor1 rapidly and processively elongates actin filaments in the presence of CrPRF

To directly examine the effect of CrPRF on CrFor1-mediated actin assembly, we visualized the assembly of 1 µM Mg-ATP actin (10% Alexa 488-labeled) over time using TIRF microscopy. Actin filaments alone (control) elongate at a rate of 11.5 subunits per second (Fig. 4A). In the presence of 1 nM CrFor1(3P,FH2), two populations of filaments were observed: actin filaments elongating at the control rate (9.1 sub/s, red arrowheads), and actin filaments elongating at a significantly slower rate (0.3 sub/s, blue arrowheads) (Fig. 4B). We interpret that the slow-growing filaments are bound at their barbed end by CrFor1, which inhibits their elongation, while filaments elongating at the control rate are not bound by CrFor1 (Kovar et al., 2003, Kovar et al., 2006). In the presence of 1 nM CrFor1 and 2.5 µM CrPRF, two distinct populations of filaments are again observed: actin filaments elongating at a rate slower than the control rate (4.2 sub/s) and rapidly elongating actin filaments (63.2 sub/s) (Fig. 4C). The assembly rate of internal control filaments is slower in these reactions because CrPRF inhibits actin filament elongation (Fig. 1B), while CrFor1 can efficiently utilize CrPRF-bound actin to rapidly elongate actin filaments. The 200-fold difference in elongation rate for CrFor1 in the absence (~0.3 sub/s) and presence of CrPRF (~60 sub/s) is one of the largest observed (Kovar, 2006).

Our results suggest that CrFor1 and CrPRF cooperate to rapidly elongate F-actin. In order to directly visualize and confirm this finding, we made a SNAP-tagged construct of CrFor1(3P,FH2) that was labeled red (549 nm) for multi-color TIRF microscopy experiments (Fig. 5). In the absence of CrPRF, red-CrFor1 remains continuously associated with the barbed end of small, slow growing actin filaments (Fig. 5A, blue arrowheads), consistent with our finding that CrFor1 can nucleate actin filaments but significantly slows actin filament elongation. Conversely, in the presence

of CrPRF, red-CrFor1-associated actin filaments elongate rapidly (Fig. 5B,D) compared to control filaments (Fig. 5C).

CrPRF favors formin- over Arp2/3 complex-mediated assembly.

We found that CrPRF potently prevents spontaneous actin assembly by both inhibiting nucleation and barbed end elongation, whereas CrFor1 overcomes this inhibition and facilitates the assembly of rapidly elongating actin filaments. In addition to enhancing formin-mediated elongation, profilin has also been shown to tune F-actin network formation by inhibiting Arp2/3 complex-mediated actin filament branch formation (Rotty et al., 2015; Suarez et al., 2015). We speculated that CrPRF might be a particularly potent inhibitor of Arp2/3 complex by inhibiting both branch formation and subsequent elongation. We tested this possibility by performing biomimetic assays in which fission yeast Arp2/3 complex activator Wsp1 or formin CrFor1 are attached to a polystyrene bead within a standard TIRF microscopy chamber (Fig. 6A,C, Movie 1). Actin alone and CrPRF-bound actin were subsequently flowed sequentially into the microscopy chamber to assess the effect of CrPRF on formin- and Arp2/3 complex-mediated actin assembly. CrFor1-bound beads poorly assembled F-actin in the absence of profilin (Fig. 6D(1), E(1)), similar to what we observed in standard TIRF microscopy assays (Fig. 4C, 5A). Addition of actin with CrPRF into the TIRF chamber triggered rapid actin filament assembly (Fig. 6D(2), E(2)). Photobleaching the rapidly assembling F-actin showed a reoccurrence of high fluorescence at the bead (Fig. 6D(3), F), indicative of rapid actin filament assembly by CrFor1 at the bead surface. Conversely, beads coated with Wsp1 assembled branched actin filaments normally following incubation with actin and Arp2/3 complex (Fig. 6A(1), E(1)). However, filament growth was halted following addition of new actin and Arp2/3 complex with CrPRF (Fig. 6B(2), E(2)). Photobleaching of F-actin revealed very little new F-actin assembly at barbed ends, consistent with CrPRF inhibition of actin filament elongation. In addition, very little F-actin assembly occurs at the bead, demonstrating inhibition of Arp2/3 complex-mediated branch formation at the bead surface (Fig. 6B(3), F).

Fertilization tubule formation is prevented by the formin inhibitor SMIFH2

CrPRF is a potent inhibitor of actin filament nucleation and elongation. However, CrPRF-bound actin can be rapidly assembled by CrFor1. We were interested in the role that this tailored protein interaction may play in facilitating actin polymerization *in vivo*. As the fertilization tubule is known to be F-actin rich and appears by EM to contain a parallel array of linear actin filaments in *Chlamydomonas* (Detmers et al., 1983), we suspected that CrFor1 might assemble the long actin filaments required for fertilization tubule formation in *Chlamydomonas* gametes. To test this, we chemically induced fertilization tubule formation in gametes and stained cells with fluorescent phalloidin to label F-actin (Fig. 7B-H). Induced gametes and 1% DMSO treated controls showed fertilization tubules in ~43% of cells (Fig. 7B, C and H). As expected, treatment with 10 µM latrunculin B, which depolymerizes F-actin networks, eliminated fertilization tubules (Fig. 7D, H).

Formin inhibitor SMIFH2 potently inhibited CrFor1-mediated actin assembly *in vitro* (Fig. 7A) (Rizvi et al., 2009). Correspondingly, though 10 µM of formin inhibitor SMIFH2 had little effect on tubule formation (Fig. 7E, H), only 5% of gametes formed fertilization tubules in the presence of 100 µM SMIFH2 (Fig. 7F, H). To confirm that fertilization tubule loss with 100 µM SMIFH2 is specific, we also treated cells with 100 µM of Arp2/3 complex inhibitor CK-666 (Nolen et al., 2009). Similar to controls, ~40% of CK-666 cells formed fertilization tubules (Fig. 7G, H), indicating that CrFor1-mediated but not Arp2/3-mediated F-actin assembly is required for fertilization tubule formation. Lastly, we found that CrFor1 is capable of bundling actin filaments to a similar extent as fission yeast formin Fus1, the formin involved in mating projectile formation in fission yeast cells (Fig. S1), suggesting that in addition to assembling actin filaments, CrFor1 could potentially also be involved in bundling of actin filaments in the fertilization tubule.

Discussion

CrPRF as a regulator of F-actin assembly

We found that, unlike typical profilins that inhibit only nucleation of new actin filaments, CrPRF is an unusual profilin, which, at relatively low concentrations, dramatically prevents unwanted actin assembly by inhibiting both the nucleation of new actin

filaments and the elongation of pre-existing actin filaments. This effect on actin filament elongation is likely due to an enhanced affinity for the barbed end, likely the result of a decreased k_{off} of CrPRF for the barbed end. Though CrPRF inhibits barbed end elongation at equimolar concentrations (Fig. 1B), other profilins have also been shown to similarly decrease barbed end elongation at 5-10-fold higher profilin concentrations (Pernier et al., 2016).The enhanced affinity of CrPRF for the barbed end could make it an ideal tool to study the mechanism and importance of profilin's competition with other barbed end ABPs (Pernier et al., 2016) such as formin, capping protein, gelsolin, and Ena/VASP. As CrPRF inhibits nucleation, elongation, and the ADP-to-ATP exchange of bound actin monomers (Kovar et al., 2001), CrPRF is an ideal regulator of the actin monomer pool, inhibiting spontaneous actin filament assembly in the cell.

Though CrPRF prevents spontaneous actin assembly, CrFor1 overcomes the inhibitory effect of CrPRF and utilizes CrPRF-bound actin to rapidly assemble actin filaments for the fertilization tubules in mating gametes. We have previously shown that the profilin defines the rate of formin-mediated actin assembly (Neidt et al., 2009). The presence of tailored formin-profilin pairs (Bestul et al., 2015) suggests that this interaction is crucial for controlling utilization of an actin monomer pool. The *Chlamydomonas* profilin CrPRF appears to be an extreme example of this, as CrPRF-bound actin does not nucleate or elongate well in the absence of CrFor1. In more complex organisms, the presence of multiple profilin isoforms expressed at different levels could regulate network size by controlling actin utilization by different formin isoforms (Mouneimne et al., 2012).

Conversely, CrPRF inhibits Arp2/3 complex-mediated actin assembly (Fig. 6). Inhibition of Arp2/3 complex-mediated branch formation and elongation could further bias *Chlamydomonas* towards CrFor1-mediated assembly, by preventing competition for actin monomers (Suarez and Kovar, 2016; Suarez et al., 2015). *Chlamydomonas* expresses components of the Arp2/3 complex, but its activators have not been identified (Kollmar et al., 2012). The Arp2/3 complex may be involved in assembly and maintenance of the F-actin involved in flagellar membrane or protein trafficking, as treatment with Arp2/3 complex inhibitor CK-666 induces flagellar shortening (Avasthi et

al., 2014). The presence of multiple potential F-actin networks provides the additional possibility that other F-actin assembly factors are also present in *Chlamydomonas*.

In addition to regulating a balance between CrFor1 and Arp2/3 mediated F-actin assembly, CrPRF also likely regulates both conventional actin and NAP1 dynamics. Of the 21 actin residues contacting profilin (Schutt et al., 1993), 15 are conserved in NAP1 and an additional three are strongly similar amino acid substitutions. Both SMIFH2 (data not shown) and CK-666 (Avasthi et al., 2014) affect flagellar length in mutants lacking conventional actin in which NAP1 is upregulated. This suggests that both formin and Arp2/3 can nucleate NAP1 filaments. Unlike SMIFH2 and CK-666, latrunculin and cytochalasin do not affect NAP1, which may explain why those treatments do not inhibit cytokinesis. Future work will involve determining the nature of the F-actin networks involved in cytokinesis and flagellar protein trafficking as well as CrPRF's role in ensuring proper F-actin distribution to each network.

CrFor1 in fertilization tubule formation

CrFor1 appears to be required for fertilization tubule formation as treatment with the formin inhibitor SMIFH2 prevents the formation of fertilization tubules. Fertilization tubule formation in *Chlamydomonas* occurs near the membrane at a site between the two flagella. Prior to fertilization tubule formation, this site is characterized by two parallel electron-dense regions called the membrane zone (immediately adjacent to the membrane) and doublet zone (slightly interior) (Detmers et al., 1983; Goodenough and Weiss, 1975). In a mature fertilization tubule, the pointed ends of actin filaments are attached at the doublet zone (Detmers et al., 1983) while the membrane zone is present at the far end of the extended fertilization tubule, near the F-actin barbed ends. As formins are typically membrane-anchored, CrFor1 is potentially localized to the membrane zone, which extends from the doublet zone following F-actin formation. Fertilization tubules are capable of partially forming in the presence of cytochalasin D (Detmers et al., 1983), suggesting that actin polymerization is specifically important for extended formation and maturation of the fertilization tubule. CrFor1 could additionally be important for bundling the actin filaments in the fertilization tubule (Fig. S1), creating

a stable projection. Future work will involve determining the factors that regulate CrFor1 activity and other ABPs that are involved in proper organization of F-actin at that site.

ACKNOWLEDGEMENTS

We thank Susan Dutcher (Washington University in St. Louis) and Bill Snell (UT Southwestern) for helpful discussions, including confirmation that *Chlamydomonas* expresses CrFor1. We thank Megan Rhyne (University of Tennessee, Knoxville) for helpful comments. This work was supported by National Institutes of Health grants R01 GM079265 (to D.R.K.), P20 GM104936 (to P.A.), NSF Graduate Student Fellowship DGE-1144082 (to J.R.C.), Molecular and Cellular Biology Training Grant T32 GM007183 (to J.R.C. and C.T.S.), and MSTP Training Grant T32GM007281 (to M.J.G.).

COMPETING INTERESTS

The authors declare no competing interests.

AUTHOR CONTRIBUTIONS

Conceptualization: JRC, MJG, LJM, PA, DRK; Methodology: JRC, MJG, LJM, DRK, PA; Data collection and analysis: JRC, MJG, DMM, YL, JAS, CTS; Writing-original draft preparation: JRC, MG, PA; Writing-reviewing and editing: JRC, DMM, PA, DRK; Funding acquisition: JRC, DRK, PA; Resources: LJM, DRK, PA; Supervision: DRK, PA.

METHODS

Plasmid construction

Constructs containing different components of the formin actin assembly domains (FH1 and FH2) were prepared for bacterial expression. The preparation of Cdc12(FH1FH2) and Cdc12(FH1) constructs has been described (Neidt et al., 2009). The CrFor1 domain constructs were designed based on sequence analysis of the *Chlamydomonas* genome, and Expressed Sequence Tag analysis by Susan Dutcher (Washington University, St.

Louis), and were optimized for bacterial expression and custom synthesized (DNA 2.0, Newark, California). Constructs were designed by SnapGene software (from GSL Biotech; available at snapgene.com). All constructs were prepared by standard cloning procedures, consisting of PCR amplification (iProof, Bio-Rad Laboratories) from the commercially prepared DNA. Restriction enzyme cleavage sites and 6x His sequences were included in the reverse primers. PCR products were cloned using restriction enzymes into pET21a (EMD Biosciences) for expression. All amplified sequences were confirmed by sequencing.

Protein purification

All constructs of CrFor1 and CrPRF were expressed in BL21-Codon Plus (DE3)-RP (Agilent Technologies, Santa Clara, CA). Cdc12(FH1FH2) (Kovar and Pollard, 2004), SpPRF (Lu and Pollard, 2001), SpFus1 (Scott et al., 2011), and CrPRF (Kovar et al., 2001) were purified as described previously. CrFor1 constructs were His-tag affinity purified. CrFor1 constructs were expressed with 0.5 mM isopropyl ß-D-thiogalactopyranoside (IPTG; Sigma-Aldrich) for 16 hours at 16°C. Cells were resuspended in extraction buffer (50 mM NaH_2PO_4, pH 8.0, 500 mM NaCl, 10% glycerol, 10 mM imidazole, 10 mM betamercaptoethanol [ßME]) supplemented with 0.5 mM phenylmethylsulfonyl fluoride (PMSF) and protease inhibitors, sonicated, and homogenized in an Emulsiflex-C3 (Avestin, Ottawa, ON, Canada). The homogenate was spun and clarified at 30,000*g* for 15 minutes, then 50,000*g* for 30 minutes and incubated with Talon Metal Affinity Resin (Clontech, Mountain View, CA) for 1 hour at 4°C. The resin was loaded onto a disposable column and washed with 50 mL wash with extraction buffer. CrFor1 was then eluted with Talon elution buffer (50 mM NaH_2PO_4, pH 8.0, 500 mM NaCl, 10% glycerol, 250 mM imidazole, 10 mM ßME) and dialyzed into formin buffer (20 mM HEPES, pH 7.4, 1 mM EDTA, 200 mM KCl, 0.01% NaN3, and 1 mM DTT).

A_{280} of purified proteins was taken using a Nanodrop 2000c Spectrophotometer (Thermo-Scientific, Waltham, MA). Protein concentrations were determined based on extinction coefficients estimated from amino acid sequences using ProtParam (http://web.expasy.org/protparam/), or from previous studies: CrPRF: 19,190 M^{-1} (Kovar

et al., 2001), SpPRF: 20,065 M^{-1} (Lu and Pollard, 2001), CrFor1(FH1,FH2): 29,450 M^{-1}, CrFor1(3P,FH2): 24,200 M^{-1}, CrFor1(FH2): 24,400 M^{-1}, SNAP-CrFor1(3P,FH2): 44,920 M^{-1}, and Cdc12 (FH1,FH2): 51,255 M^{-1} (Kovar et al., 2003). Protein concentrations of FH1 constructs Cdc12(FH1), CrFor1(FH1) , and CrFor1(3P) were determined by A_{205} in water ([(A_{205}FH1− A_{205}buffer)/30]/mol wt). Proteins were flash-frozen in liquid nitrogen and kept at -80°C. SNAP-CrFor1(3P,FH2) protein was labeled with SNAP-549 dye (New England Biolabs, Ipswich, MA) as per manufacturer's instructions prior to each TIRF experiment.

Actin was purified from rabbit or chicken skeletal muscle actin as previously described (Spudich and Watt, 1971). For pyrene assembly assays, actin was labeled with N-(1-Pyrene)Iodoacetamide (Life Technologies, Carlsbad, CA) on Cys-374. As the combination of CrFor1 in the presence of CrPRF selected against actin labeled on Cys-374, actin labeled with Alexa Fluor 488 on lysines (ThermoFisher Scientific, Waltham, MA) was used for TIRF microscopy experiments.

Pyrene assembly and disassembly assays

All pyrene assembly and disassembly assays were carried out in a 96-well plate, and the fluorescence of pyrene-actin (excitation at 364 nm and emission at 407 nm) was measured with a Spectramax Gemini XPS (Molecular Devices) or Safire2 (Tecan) fluorescent plate reader as described (Zimmermann et al., 2016). For spontaneous assembly assays, a 15 µM mixture of 20% pyrene-labeled Mg-ATP-actin monomer with 100X anti-foam 204 (0.005%; Sigma) was placed in the upper well of a 96 well non-binding black plate. Formin and/or profilin, 10X KMEI (500 mM KCl, 10 mM $MgCl_2$, 10 mM ethylene glycol tetraacetic acid [EGTA], and 100 mM imidazole, pH 7.0), and Mg-Buffer G (2 mM Tris, pH 8.0, 0.2 mM ATP, 0.1 mM MgCl2 and 0.5 mM DTT) were placed in the lower row of the plate. Reactions were initiated by mixing contents of the lower wells the actin monomers in the upper wells with a twelve-channel pipetman (Eppendorf). For pyrene assembly assays involving SMIFH2, SMIFH2 was added to the lower wells containing CrFor1 prior to mixing the upper and lower wells.

For seeded assembly assays, 5.0 µM unlabeled Mg-ATP-actin was preassembled in the upper row of the plate, followed by addition of anti-foam, formin

and/or profilin, and Mg-Buffer G. A 2.0 µM mixture of 20% pyrene-labeled actin with Mg-Buffer G was placed in the lower plate row. Mixing actin monomers in lower wells with pre-assembled actin filaments in upper wells initiated reactions.

For depolymerization assays, a 5.0 µM mixture of unlabeled and 50% pyrene-labeled Mg-ATP-actin monomers was preassembled in the upper row of the plate for two hours, followed by addition of anti-foam. Formin, 10X KMEI and Mg-Buffer G were placed in the lower plate row. Reactions were initiated by mixing lower wells with upper wells, diluting the pre-assembled filaments to 0.1 µM.

Profilin FH1 affinity assays

The affinity of profilin for formin(FH1) was determined by measuring the change in profilin's intrinsic tryptophan fluorescence by excitation at 295 nm and emission at 323 nm (Perelroizen et al., 1994; Petrella et al., 1996). Profilin (1.0 µM) was incubated with a range of poly-L-proline or formin(FH1) concentrations for 30 min, then profilin fluorescence was read in a Safire2 fluorescence plate reader and plotted versus formin(FH1) concentration. The fluorescence of formin(FH1) alone was subtracted from the fluorescence in the presence of profilin. Dissociation constants (K_d) were determined by fitting a quadratic function to the dependence of the concentration of bound profilin on the concentration of formin(FH1).

Polymerization and depolymerization rate determination

Actin assembly rates were determined from spontaneous assembly reactions by measuring the slopes of actin assembly following the lag phase to 50% of total actin assembly. Assembly rates from preassembled actin seeds were determined by a linear fit to the first 100 seconds of assembly. Depolymerization rates were determined by a linear fit to the first 100-300 seconds of the reaction.

The affinity of CrFor1 for barbed ends was determined as previously described (Kovar *et al.*, 2003). We fit the plot of the dependence of the assembly or disassembly rate on formin concentration using the equation $V_i = V_{if} + (V_{ib} - V_{if})$ $((K_d + [\text{ends}] + [\text{formin}] - \sqrt{((K_d + [\text{ends}] + [\text{formin}])2 - 4[\text{ends}][\text{formin}])/2[\text{ends}]}))$, where V_i is the observed elongation or depolymerization rate, V_{if} is the elongation or depolymerization

rate of free barbed ends, V_{ib} is the elongation or depolymerization rate of bound barbed ends, [ends] is the concentration of barbed ends, and [formin] is formin concentration. The nucleation efficiency was calculated by dividing the slope of the spontaneous assembly rate by *k*+ in the absence and presence of profilin and dividing by the formin concentration (Kovar et al., 2006). Depolymerization rates are normalized to the rate of actin assembly alone and expressed as a percent of the standard actin assembly rate.

Fluorescence micrographs (rhodamine phalloidin)

Unlabeled Mg-ATP-actin was assembled as per standard spontaneous assembly reactions. Actin filaments were then incubated with 1 µM TRITC-Phalloidin (Fluka Biochemika, Switzerland) for 5 minutes. Reactions were terminated by diluting assembled filaments in fluorescence buffer (50 mM KCl, 1 mM $MgCl_2$, 100 mM DTT, 20 µg/ml catalase, 100 µg/ml glucose oxidase, 3 mg/ml glucose, 0.5% methylcellulose, and 10 mM imidazole, pH 7.0) and were absorbed to coverslips coated with 0.05 µg/µl poly-L-lysine. Fluorescence microscopy images were collected on an Olympus IX-81 microscope and cooled CCD camera (Orca-ER, Hamamatsu).

Low-speed sedimentation assays

Sedimentation assays were performed as previously described (Zimmermann et al., 2016). 15 µM Mg-ATP actin monomers were spontaneously assembled for 1 hour in 10 mM imidazole, pH 7.0, 50 mM KCl, 5 mM $MgCl_2$, 1 mM EGTA, 0.5 mM DTT, 0.2 mM ATP and 90 µM $CaCl_2$ to generate F-actin. Filamentous actin was then incubated with CrFor1 or SpFus1 for 20 minutes at 25ºC and spun at 10,000g at 25ºC. Supernatant and pellets were separated by 15% SDS-PAGE gel electrophoresis and stained with Coomassie Blue for 30 minutes, destained for 16 hours and analyzed by densitometry with ImageJ (Schneider et al., 2012; http://imagej.net).

TIRF microscopy

Time-lapse TIRF microscopy movies were obtained using a iXon EMCCD camera (Andor Technology, Belfast, UK) fitted to an Olympus IX-71 microscope with through-the-objective TIRF illumination as described (Zimmermann et al., 2016). Mg-ATP-actin

(10-20% Alexa 488-labeled) was mixed with a polymerization mix (10 mM imidazole (pH 7.0), 50 mM KCl, 1 mM MgCl2, 1 mM EGTA, 50 mM DTT, 0.2 mM ATP, 50 µM CaCl2, 15 mM glucose, 20 µg/mL catalase, 100 µg/mL glucose oxidase, and 0.5% (400 centipoise) methylcellulose) to induce F-actin assembly (Winkelman et al., 2014). Where stated, formin or profilin was added to the polymerization mix prior to mixing with actin and initiating F-actin polymerization. The mixture was then added to a flow chamber and imaged at 10 s intervals at room temperature. For bead assays, Wsp1 and formin beads were prepared as previously described (Loisel et al., 1999). Carboxylated Polybeads (Polysciences, Warrington, PA) were coated with Wsp1 or CrFor1 and flowed into the TIRF chamber prior to initiating the reaction.

Fertilization tubule assay

Wild type 137c (CC-125 mt+) *Chlamydomonas reinhardtii* cells were obtained from the Chlamydomonas Resource Center (University of Minnesota). To induce gametogenesis, cells were grown in M-N (M1 minimal media without nitrogen) overnight under growth lighting. Gametes were mixed with dibutyryl cAMP (13.5mM) and papaverine (135µM) to induce fertilization tubule formation along with different inhibitor preparations; untreated, 1% DMSO (solvent for all inhibitors), 10µM Latrunculin B, 10µM SMIFH2, 100µM SMIFH2, and 100µM CK-666. Cells were placed on a rotator under a LumiBar LED light source (LumiGrow, Inc) for 2hrs. After fertilization tubule induction, cells were adhered to coverslips coated with poly-lysine and fixed with 4% paraformaldehyde in 10mM HEPES. They were permeabilized with -20°C acetone, stained with 100nM Alexa Fluor 488 Phalloidin (Life Technologies) according to manufacturer protocols and mounted on slides with Fluoromount-G (Southern Biotech) for imaging. Slides were imaged with a Nikon Ti-S widefield fluorescence microscope using a Plan Achromat 100x/1.25 NA oil immersion objective lens, a QICam fast 1394 CCD digital camera (QImaging) and NIS Elements software.

All cells in multiple fields of view (~50-100 cells per condition) were counted for presence of fertilization tubules using the ImageJ Cell Counter plugin to determine tubule percentage (#tubules/# total cells) x 100. Means and standard deviations are plotted for experiments done in triplicate. Results were analyzed with one way ANOVA

and Dunnett's multiple comparison post hoc test. For fertilization tubule measurements, line segments were drawn onto projected FITC images and fit with splines using ImageJ. n>45 measurements were collected following a pixel to micron ratio conversion for the optical setup and compared using Kruskal-Wallis and Dunn's multiple comparison tests.

Figures

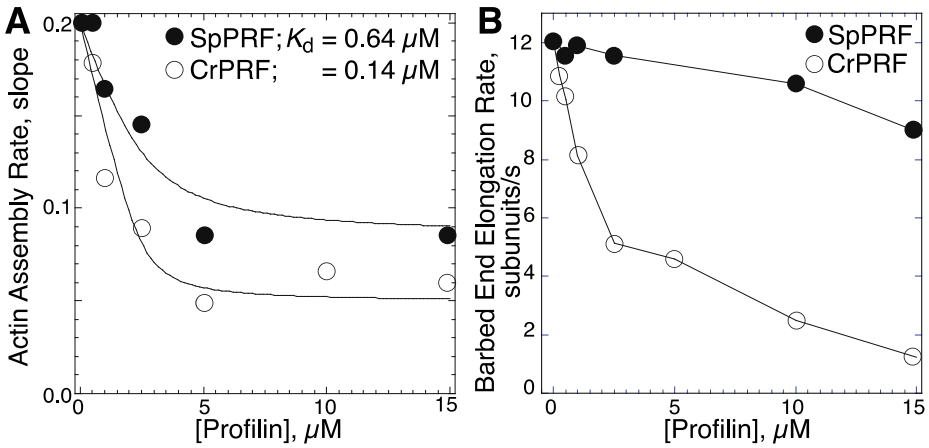

Figure 1: CrPRF inhibits nucleation and elongation of actin filaments.

(A) Slopes of spontaneous pyrene actin assembly assays (1.5 μM Mg-ATP actin, 20% pyrene labeled) with increasing concentrations of fission yeast profilin SpPRF or *Chlamydomonas reinhardtii* profilin CrPRF. Curve fits reveal affinities of SpPRF and CrPRF for actin monomer. (B) Barbed end elongation rates of 1.5 μM Mg-ATP actin (10% Alexa-488 labeled) in the presence of increasing concentrations of SpPRF or CrPRF, measured by TIRF microscopy.

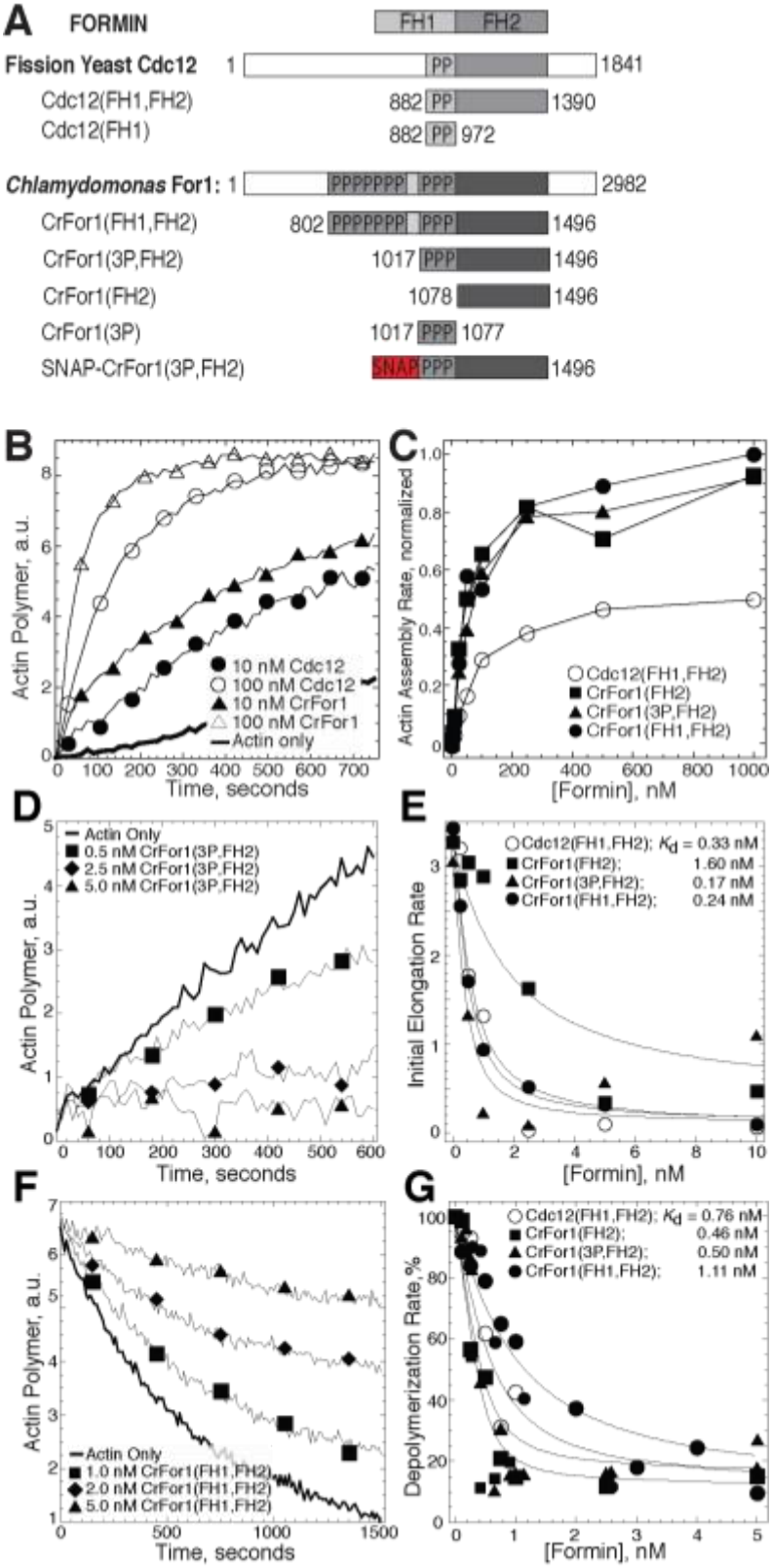

Figure 2: CrFor1 efficiently nucleates actin filaments that elongate slowly.

(A) Domain organizations and constructs used in this study of fission yeast formin Cdc12 and *Chlamydomonas reinhardtii* formin CrFor1. Numbers denote amino acid residues. Each "P" indicates a putative profilin binding site of at least 6 prolines within 8 residues. (B and C) Spontaneous assembly of 2.5 *μ*M Mg-ATP actin monomers (20% pyrene labeled). (B) Pyrene fluorescence over time for actin alone (thick curve), and with 10 (●) or 100 nM (○) Cdc12(FH1,FH2) or 10 (▲) and 100 nM (△) CrFor1(3P,FH2). (C) Dependence of the normalized actin assembly rate (slope) on the concentration of Cdc12(FH1,FH2) (○), CrFor1(FH2) (■), CrFor1(3P,FH2) (▲), and CrFor1(10P,FH2) (●). (D and E) Seeded assembly of 0.2 *μ*M Mg-ATP actin monomers (20% pyrene labeled) onto 0.5 μM preassembled filaments. (D) Pyrene fluorescence over time for actin alone (thick line) or in the presence of 0.5 (□), 1.0 (◆), or 2.5 nM (▲) CrFor1(3P,FH2). (E) Dependence of the initial barbed end assembly rate on formin concentration. Curve fits revealed equilibrium dissociation constants of 0.33 nM for Cdc12(FH1,FH2) (○), 1.6 nM for CrFor1(FH2) (■), 0.17 nM for CrFor1(3P,FH2) (▲), and 0.24 nM for CrFor1(10P,FH2) (●). (F and G) F-actin disassembly assays: depolymerization of 5 μM actin filaments (50% pyrene labeled) after dilution to 0.1 μM. (F) Depolymerization time-course in the absence (thick curve) or presence of 0.1 (□), 0.25 (◆), or 0.5 nM (▲) CrFor1(3P,FH2). (F) Dependence of the depolymerization rate on the concentration of the indicated formin. Curve fits revealed equilibrium dissociation constants of 0.76 nM for Cdc12(FH1,FH2) (○), 0.46 nM for CrFor1(FH2) (□), 0.50 nM CrFor1(3P,FH2) (▲), and 1.11 nM for CrFor1(10P,FH2) (●).

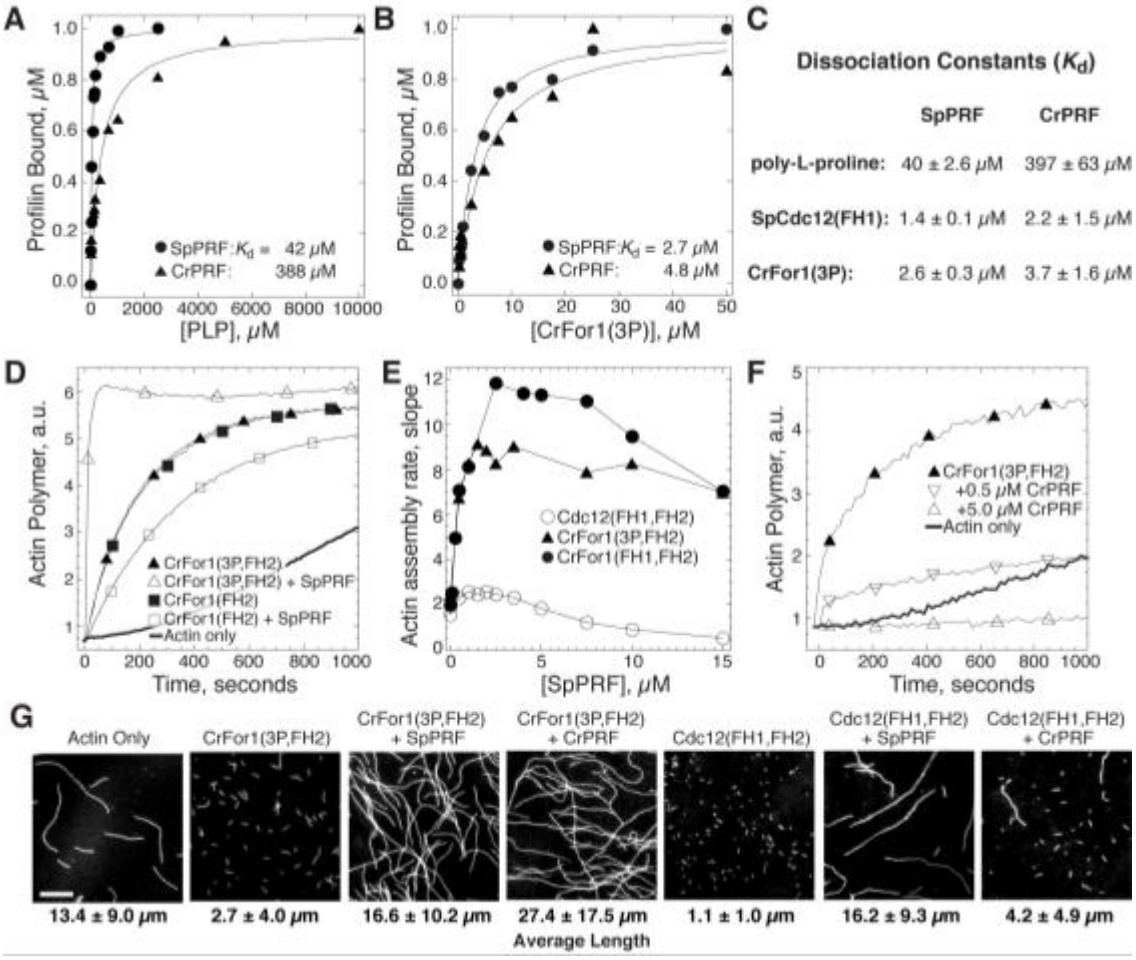

Figure 3: CrFor1 stimulates the assembly of profilin-actin. (A-C) Affinity of profilin for poly-L-proline and formin FH1 domains. Dependence of fission yeast SpPRF (•) and CrPRF (▲) intrinsic tryptophan fluorescence on the concentration of poly-L-proline (A) and CrFor1(3P) (B). (C) Average affinity of SpPRF and CrPRF for poly-L-proline, Cdc12(FH1) and CrFor1(3P); n≥3 experiments. (D-F) Spontaneous assembly of 2.5 μM Mg-ATP actin (20% pyrene-labeled). (D) Pyrene fluorescence over time for actin alone (thick curve), and with 10 nM CrFor1(FH2) in the absence (□) or presence (□) of 2.5 μM SpPRF, and with 10 nM CrFor1(3P,FH2) in the absence (▲) or presence (△) of 2.5 μM SpPRF. (E) Dependence of the actin assembly rate (slope) on the concentration of SpPRF for reactions containing 10 nM CrFor1(3P,FH2) (▲) or 10 nM Cdc12(FH1,FH2) (•). (F) Pyrene fluorescence over time for actin alone (thick curve), and with 10 nM CrFor1(3P,FH2) in the absence (▲), or presence of 0.5 μM (▽), or 5.0 μM (△) CrPRF.

667 (G) Fluorescence micrographs of actin filaments taken 10 minutes after the initiation of
668 the indicated reactions with 10 nM formin and 2.5 µM profilin. Samples were labeled
669 with rhodamine-phalloidin and adsorbed to glass coverslips coated with poly-L-lysine.
670 Scale bar, 5 µm.
671

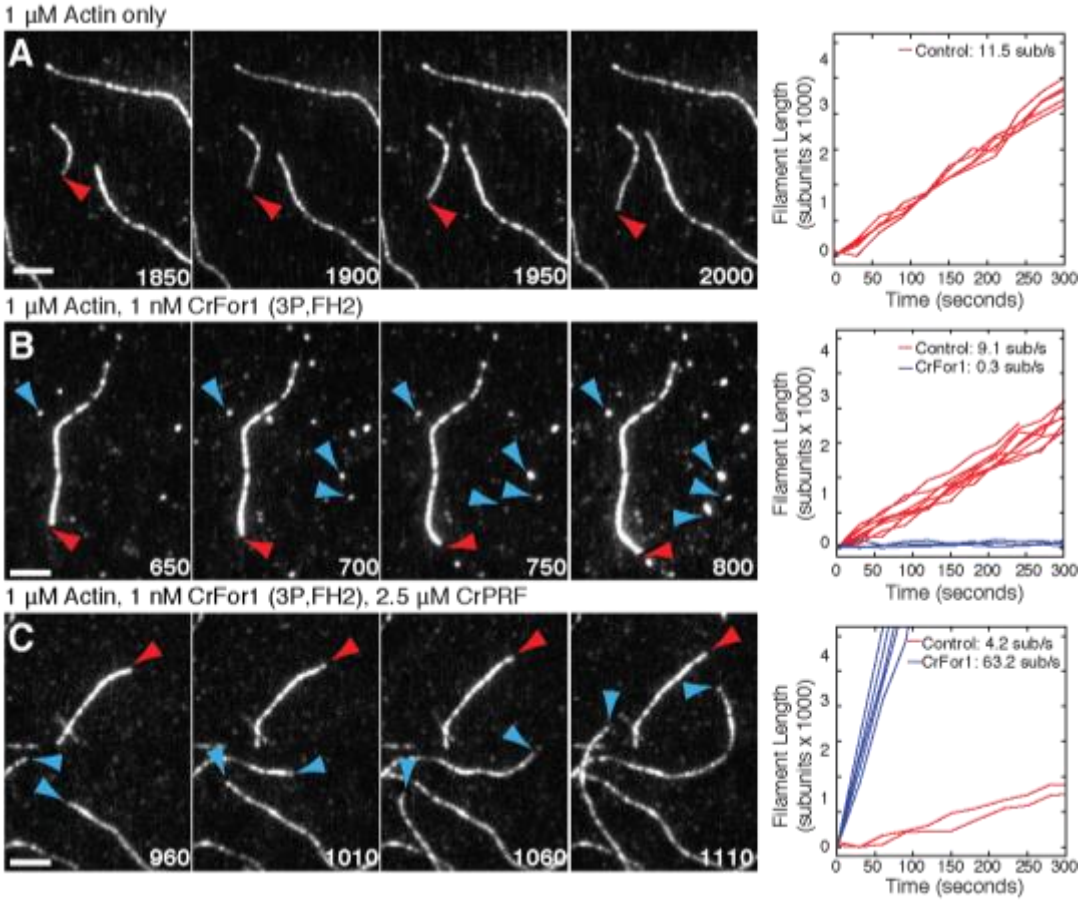

Figure 4: CrFor1 rapidly elongates actin filaments in the presence of CrPRF.

(A-C) TIRF microscopy of 1 µM Mg-ATP actin (20% Alexa 488-labeled). (Left) Time lapse micrographs with time in seconds of actin alone **(A)**, with CrFor1(3P,FH2) **(B)**, and with CrFor1(3P, FH2) and CrPRF. Red and blue arrowheads denote control (formin independent) and CrFor1-dependent filaments, respectively. Scale bars, 5 µm. (Right) Rates of filament growth for control (red lines) and CrFor1-associated (blue lines) filaments.

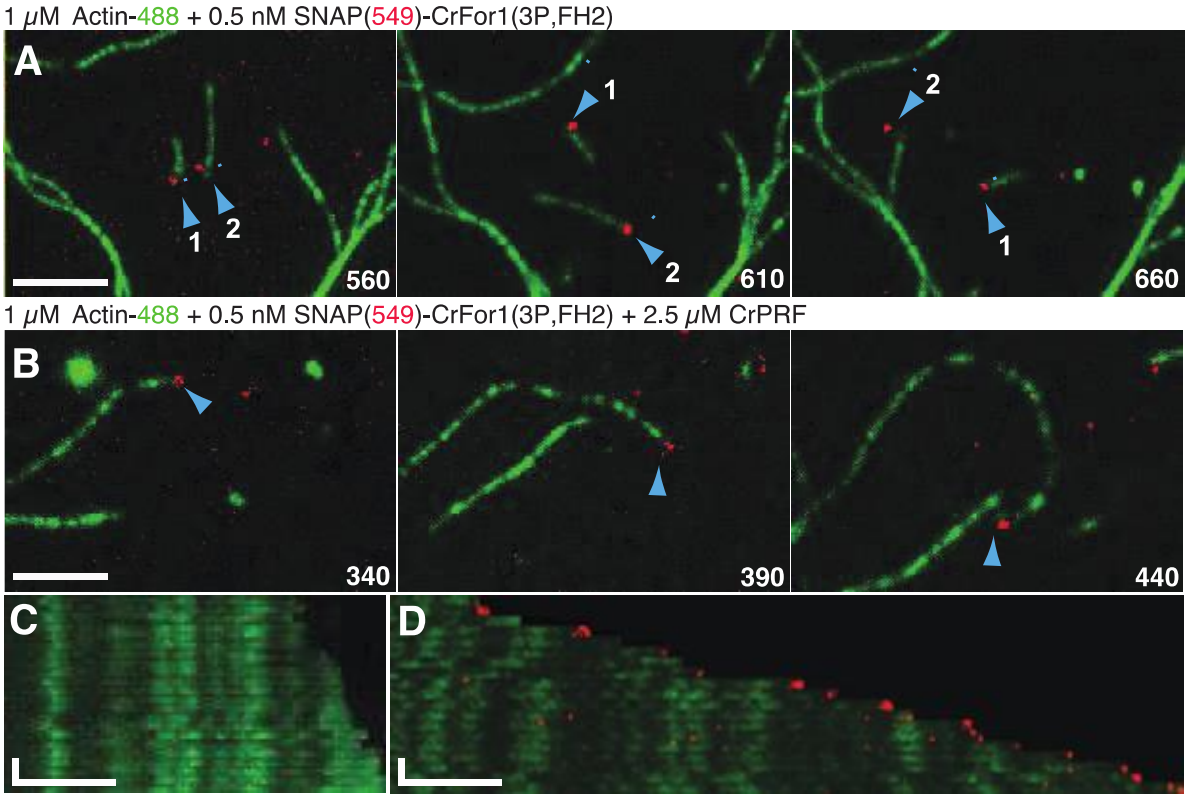

Figure 5: CrFor1 is processive in the absence and presence of CrPRF.

(A-D) Two-color TIRF microscopy of 1 μM Mg-ATP actin (10% Alexa 488-labeled) with 0.5 μM SNAP-CrFor1(3P,FH2) (549-labeled) in the presence or absence of 2.5 μM CrPRF. Blue arrowheads denote formin-bound filaments. **(A)** 0.5 μM SNAP-CrFor1(3P,FH2) alone. **(B)** 0.5 μM SNAP-CrFor1(3P,FH2) in the presence of 2.5 μM CrPRF. **(C and D)** Kymographs of control **(C)** and formin-bound **(D)** filaments from **(B)**. Scale bars, x-axis, 5 μm. Time bars, y-axis, 30 sec.

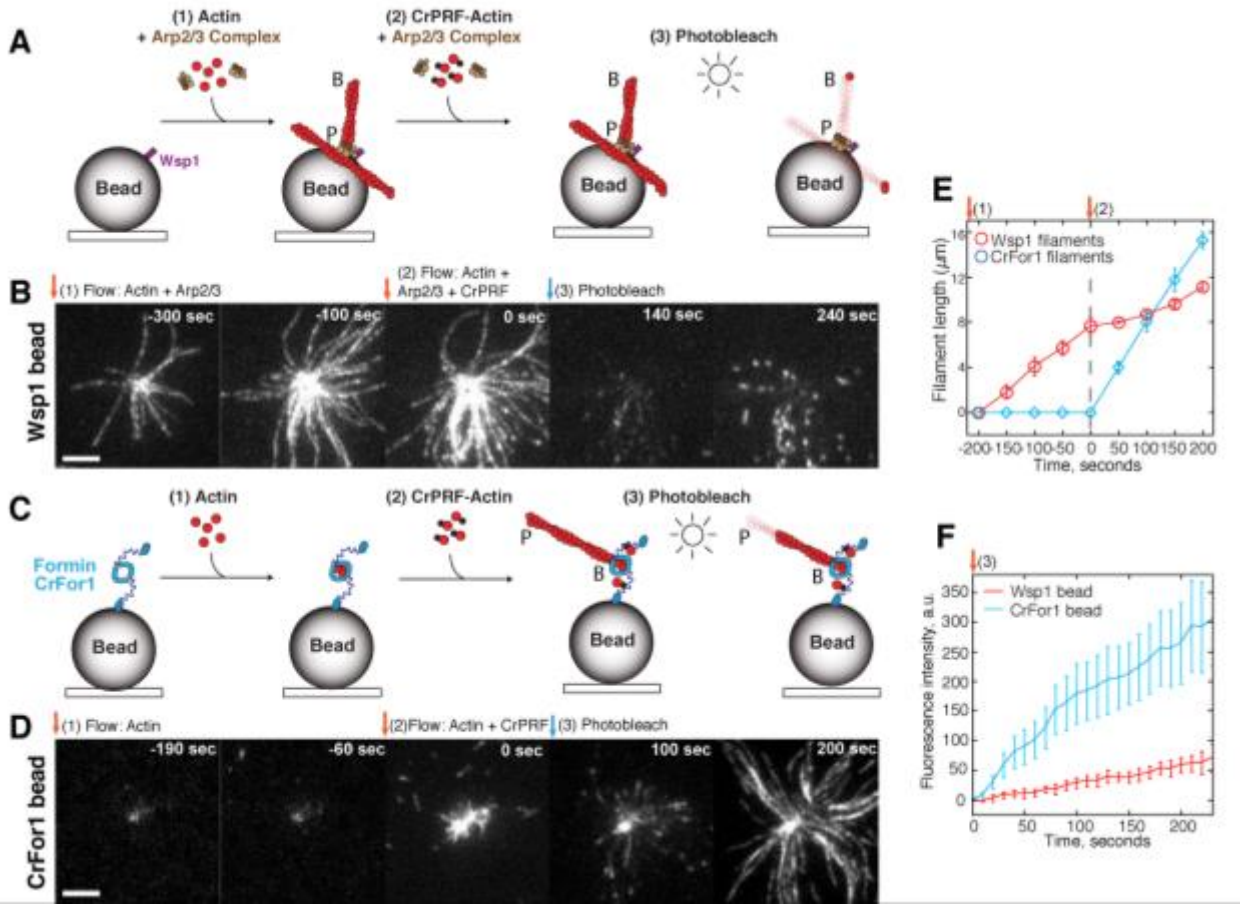

Figure 6: CrPRF facilitates formin- over Arp2/3 complex-mediated assembly.

(A-F) TIRF microscopy bead assays. Fission yeast Arp2/3 complex activator Wsp1 or formin CrFor1 are adsorbed to a polystyrene bead and the effect of CrPRF-actin on network formation is observed. ‘B’ and 'P' indicate actin filament barbed and pointed ends, respectively. **(A-B)** Reactions containing beads coated with Wsp1. 1.5 μM Mg-ATP actin (10% Alexa 488-labeled) and 30 nM Arp2/3 complex is initially flowed into the chamber (1), followed by actin, Arp2/3 complex, and 2.5 μM CrPRF (2). Filaments are then photobleached to observe new assembly (3). **(C-D)** Reactions containing beads coated with CrFor1. Actin is initially flowed into the chamber (1), followed by actin and CrPRF (2), and then photobleached (3). **(E)** Actin filament length over time for filaments associated with Wsp1 (red) or CrFor1 (blue) beads. The initial flow of actin (1) and then actin with CrPRF (2) are indicated. Value reported is mean ± s.e.m., n=5 filaments. **(F)** Quantification of fluorescence intensity (actin assembly) at the surface of a Wsp1-coated (red) or CrFor1-coated (blue) beads following flow-in of CrPRF-actin and

719 photobleaching. Each experiment was replicated twice. Value reported is mean ±
720 s.e.m., n=3 Wsp1 or n=4 CrFor1 beads.

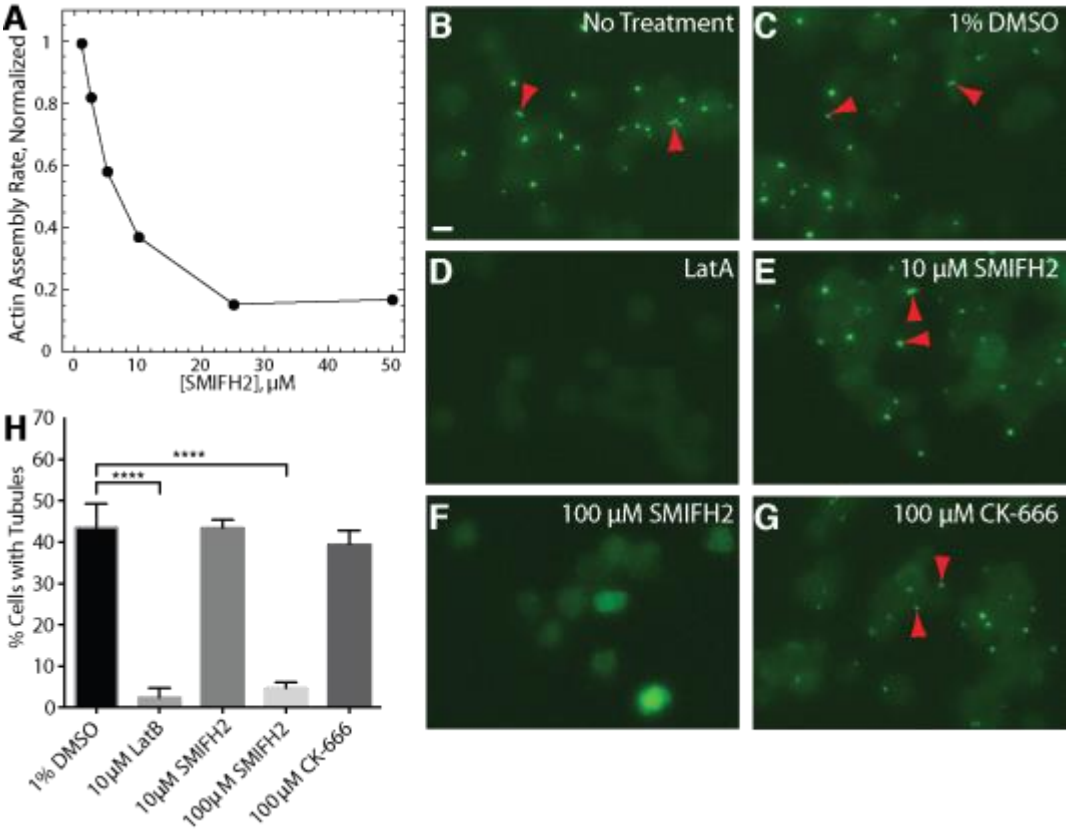

Figure 7: SMIFH2 formin inhibition disrupts fertilization tubules in *Chlamydomonas* gametes

(A) Normalized actin assembly rate of CrFor1(3P,FH2) (●) in the presence of increasing concentrations of formin inhibitor SMIFH2. **(B-F)** Representative fluorescent micrographs of *Chlamydomonas* gamete fertilization tubules (red arrowheads) labeled with the F-actin marker 488-phalloidin. Scale bar, 10 µm. **(B)** Untreated control. **(C)** 1% DMSO control. **(D)** 10 µM actin depolymerization drug Latrunculin B. **(E)** 10 µM formin inhibitor SMIFH2. **(F)** 100 µM SMIFH2. **(G)**100 µM Arp2/3 complex inhibitor CK-666. **(H)** Quantification of the percent of cells with fertilization tubules following indicated treatments. n=3 independent experiments. Values reported are mean ± s.d., ****p<0.0001.

REFERENCES

Avasthi, P., Onishi, M., Karpiak, J., Yamamoto, R., Mackinder, L., Jonikas, M. C., Sale, W. S., Shoichet, B., Pringle, J. R. and Marshall, W. F. (2014). Actin Is Required for IFT Regulation in Chlamydomonas reinhardtii. *Current Biology* **24**, 2025–2032.

Bestul, A. J., Christensen, J. R., Grzegorzewska, A. P., Burke, T. A., Sees, J. A., Carroll, R. T., Sirotkin, V., Keenan, R. J. and Kovar, D. R. (2015). Fission yeast profilin is tailored to facilitate actin assembly by the cytokinesis formin Cdc12. *Mol. Biol. Cell* **26**, 283–293.

Breitsprecher, D. and Goode, B. L. (2013). Formins at a glance. *J. Cell. Sci.* **126**, 1–7.

Carlsson, L., Nystrom, L. E., Sundkvist, I., Markey, F. and Lindberg, U. (1977). Actin polymerizability is influenced by profilin, a low molecular weight protein in non-muscle cells. *Journal of Molecular Biology* **115**, 465–483.

Detmers, P. A., Carboni, J. M. and Condeelis, J. (1985). Localization of actin in Chlamydomonas using antiactin and NBD-phallacidin. *Cell Motil.* **5**, 415–430.

Detmers, P. A., Goodenough, U. W. and Condeelis, J. (1983). Elongation of the fertilization tubule in Chlamydomonas: new observations on the core microfilaments and the effect of transient intracellular signals on their structural integrity. *The Journal of Cell Biology* **97**, 522–532.

Goldschmidt-Clermont, P. J., Kim, J. W., Machesky, L. M., Rhee, S. G. and Pollard, T. D. (1991). Regulation of phospholipase C-gamma 1 by profilin and tyrosine phosphorylation. **251**, 1231–1233.

Goodenough, U. W. and Weiss, R. L. (1975). Gametic differentiation in Chlamydomonas reinhardtii. III. Cell wall lysis and microfilament-associated mating structure activation in wild-type and mutant strains. *The Journal of Cell Biology* **67**, 623–637.

Harper, J. D., McCurdy, D. W., Sanders, M. A., Salisbury, J. L. and John, P. C. (1992). Actin dynamics during the cell cycle in Chlamydomonas reinhardtii. *Cell Motil. Cytoskeleton* **22**, 117–126.

Kaiser, D. A., Vinson, V. K., Murphy, D. B. and Pollard, T. D. (1999). Profilin is predominantly associated with monomeric actin in Acanthamoeba. *J. Cell. Sci.* **112 (Pt 21)**, 3779–3790.

Kato-Minoura, T. E. A. (1998). Highly Divergent Actin Expressed in a Chlamydomonas Mutant Lacking the Conventional Actin Gene. 1–6.

Kato-Minoura, T., Hirono, M. and Kamiya, R. (1997). Chlamydomonas inner-arm dynein mutant, ida5, has a mutation in an actin-encoding gene. *The Journal of Cell*

Biology **137**, 649–656.

Kollmar, M., Lbik, D. and Enge, S. (2012). Evolution of the eukaryotic ARP2/3 activators of the WASP family: WASP, WAVE, WASH, and WHAMM, and the proposed new family members WAWH and WAML. *BMC Research Notes* **5**, 88.

Kovar, D. R. (2006). Molecular details of formin-mediated actin assembly. *Curr. Opin. Cell Biol.* **18**, 11–17.

Kovar, D. R. and Pollard, T. D. (2004). Insertional assembly of actin filament barbed ends in association with formins produces piconewton forces. *Proc Natl Acad Sci USA* **101**, 14725–14730.

Kovar, D. R., Harris, E. S., Mahaffy, R., Higgs, H. N. and Pollard, T. D. (2006). Control of the assembly of ATP- and ADP-actin by formins and profilin. *Cell* **124**, 423–435.

Kovar, D. R., Kuhn, J. R., Tichy, A. L. and Pollard, T. D. (2003). The fission yeast cytokinesis formin Cdc12p is a barbed end actin filament capping protein gated by profilin. *The Journal of Cell Biology* **161**, 875–887.

Kovar, D. R., Yang, P., Sale, W. S., Drobak, B. K. and Staiger, C. J. (2001). Chlamydomonas reinhardtii produces a profilin with unusual biochemical properties. *J. Cell. Sci.* **114**, 4293–4305.

Lee, V. D., Finstad, S. L. and Huang, B. (1997). Cloning and characterization of a gene encoding an actin-related protein in Chlamydomonas. *Gene* **197**, 153–159.

Loisel, T. P., Boujemaa, R., Pantaloni, D. and Carlier, M. F. (1999). Reconstitution of actin-based motility of Listeria and Shigella using pure proteins. *Nature* **401**, 613–616.

Lu, J. and Pollard, T. D. (2001). Profilin binding to poly-L-proline and actin monomers along with ability to catalyze actin nucleotide exchange is required for viability of fission yeast. *Molecular Biology of the Cell* **12**, 1161–1175.

Mockrin, S. C. and Korn, E. D. (1980). Acanthamoeba profilin interacts with G-actin to increase the rate of exchange of actin-bound adenosine 5'-triphosphate. *Biochemistry* **19**, 5359–5362.

Mouneimne, G., Hansen, S. D., Selfors, L. M., Petrak, L., Hickey, M. M., Gallegos, L. L., Simpson, K. J., Lim, J., Gertler, F. B., Hartwig, J. H., et al. (2012). Differential remodeling of actin cytoskeleton architecture by profilin isoforms leads to distinct effects on cell migration and invasion. *Cancer Cell* **22**, 615–630.

Neidt, E. M., Scott, B. J. and Kovar, D. R. (2009). Formin differentially utilizes profilin isoforms to rapidly assemble actin filaments. *J. Biol. Chem.* **284**, 673–684.

Nolen, B. J., Tomasevic, N., Russell, A., Pierce, D. W., Jia, Z., McCormick, C. D., Hartman, J., Sakowicz, R. and Pollard, T. D. (2009). Characterization of two classes of small molecule inhibitors of Arp2/3 complex. *Nature* **460**, 1031–1035.

Onishi, M., Pringle, J. R. and Cross, F. R. (2016). Evidence That an Unconventional Actin Can Provide Essential F-Actin Function and That a Surveillance System Monitors F-Actin Integrity in Chlamydomonas. *Genetics* **202**, 977–996.

Otomo, T., Tomchick, D. R., Otomo, C., Panchal, S. C., Machius, M. and Rosen, M. K. (2005). Structural basis of actin filament nucleation and processive capping by a formin homology 2 domain. *Nature* **433**, 488–494.

Perelroizen, I., Didry, D., Christensen, H., Chua, N. H. and Carlier, M. F. (1996). Role of nucleotide exchange and hydrolysis in the function of profilin in action assembly. *J. Biol. Chem.* **271**, 12302–12309.

Perelroizen, I., Marchand, J. B., Blanchoin, L., Didry, D. and Carlier, M. F. (1994). Interaction of profilin with G-actin and poly(L-proline). *Biochemistry* **33**, 8472–8478.

Pernier, J., Shekhar, S., Jegou, A., Guichard, B. and Carlier, M.-F. (2016). Profilin Interaction with Actin Filament Barbed End Controls Dynamic Instability, Capping, Branching, and Motility. *Dev. Cell* **36**, 201–214.

Petrella, E. C., Machesky, L. M., Kaiser, D. A. and Pollard, T. D. (1996). Structural requirements and thermodynamics of the interaction of proline peptides with profilin. *Biochemistry* **35**, 16535–16543.

Pollard, T. D. and Cooper, J. A. (1984). Quantitative analysis of the effect of Acanthamoeba profilin on actin filament nucleation and elongation. *Biochemistry* **23**, 6631–6641.

Rizvi, S. A., Neidt, E. M., Cui, J., Feiger, Z., Skau, C. T., Gardel, M. L., Kozmin, S. A. and Kovar, D. R. (2009). Identification and characterization of a small molecule inhibitor of formin-mediated actin assembly. *Chem Biol* **16**, 1158–1168.

Rotty, J. D., Wu, C., Haynes, E. M., Suarez, C., Winkelman, J. D., Johnson, H. E., Haugh, J. M., Kovar, D. R. and Bear, J. E. (2015). Profilin-1 Serves as a Gatekeeper for Actin Assembly by Arp2/3-Dependent and -Independent Pathways. *Developmental Cell* **32**, 54–67.

Schmitz, S., Grainger, M., Howell, S., Calder, L. J., Gaeb, M., Pinder, J. C., Holder, A. A. and Veigel, C. (2005). Malaria parasite actin filaments are very short. *Journal of Molecular Biology* **349**, 113–125.

Schneider, C. A., Rasband, W.S., and Eliceiri, K. W. (2012). NIH Image to ImageJ: 25 years of image analysis. *Nature Methods* **9**, 671-675.

Scott, B. J., Neidt, E. M. and Kovar, D. R. (2011). The functionally distinct fission

865 yeast formins have specific actin-assembly properties. *Mol. Biol. Cell* **22**, 3826–
866 3839.

867 **Skillman, K. M., Diraviyam, K., Khan, A., Tang, K., Sept, D. and Sibley, L. D.** (2011).
868 Evolutionarily Divergent, Unstable Filamentous Actin Is Essential for Gliding Motility
869 in Apicomplexan Parasites. *PLoS Pathog* **7**, e1002280–17.

870 **Spudich, J. A. and Watt, S.** (1971). The regulation of rabbit skeletal muscle
871 contraction. I. Biochemical studies of the interaction of the tropomyosin-troponin
872 complex with actin and the proteolytic fragments of myosin. *J. Biol. Chem.* **246**,
873 4866–4871.

874 **Suarez, C. and Kovar, D. R.** (2016). Internetwork competition for monomers governs
875 actin cytoskeleton organization. *Nat Rev Mol Cell Biol* 1–12.

876 **Suarez, C., Carroll, R. T., Burke, T. A., Christensen, J. R., Bestul, A. J., Sees, J. A.,**
877 **James, M. L., Sirotkin, V. and Kovar, D. R.** (2015). Profilin Regulates F-Actin
878 Network Homeostasis by Favoring Formin over Arp2/3 Complex. *Developmental*
879 *Cell* **32**, 43–53.

880 **Wilson, N. F., Foglesong, M. J. and Snell, W. J.** (1997). The Chlamydomonas mating
881 type plus fertilization tubule, a prototypic cell fusion organelle: isolation,
882 characterization, and in vitro adhesion to mating type minus gametes. *The Journal*
883 *of Cell Biology* **137**, 1537–1553.

884 **Winkelman, J. D., Bilancia, C. G., Peifer, M. and Kovar, D. R.** (2014). Ena/VASP
885 Enabled is a highly processive actin polymerase tailored to self-assemble parallel-
886 bundled F-actin networks with Fascin. *Proceedings of the National Academy of*
887 *Sciences of the United States of America*.

888 **Zimmermann, D., Morganthaler, A. N., Kovar, D. R. and Suarez, C.** (2016). In Vitro
889 Biochemical Characterization of Cytokinesis Actin-Binding Proteins. *Methods Mol.*
890 *Biol.* **1369**, 151–179.

891